A model for laminar diffusion-based complex electrokinetic passive micromixers

Yi Wang,[a] Qiao Lin*[a] and Tamal Mukherjee[b]

Received 5th January 2005, Accepted 8th June 2005
First published as an Advance Article on the web 6th July 2005
DOI: 10.1039/b500010f

This paper presents a model for the efficient and accurate simulations of laminar diffusion-based complex electrokinetic passive micromixers by representing them as a system of mixing elements of relatively simple geometry. Parameterized and analytical models for such elements are obtained, which hold for general sample concentration profiles and arbitrary flow ratios at the element inlet. A lumped-parameter and system-level model is constructed for a complex micromixer, in which the constituent mixing elements are represented by element models, in such a way that an appropriate set of parameters are continuous at the interface between each pair of adjacent elements. The system-level model, which simultaneously computes electric circuitry and sample concentration distributions in the entire micromixer, agrees with numerical and experimental results, and offers orders-of-magnitude improvements in computational efficiency over full numerical simulations. The efficiency and usefulness of the model is demonstrated by exploring a number of laminar diffusion based mixers and mixing networks that occur in practice.

1 Introduction

Lab-on-a-chip systems have been actively pursued and studied in the past decade, and hold great promise for a wide spectrum of applications in biology, medicine and chemistry.[1,2] Microscale mixing, especially its integration with other bio-processing functionalities such as sample preparation, reaction, injection, separation and detection,[1–4] holds great importance in lab-on-a-chip technology. It is generally desirable for micromixers to have simple designs for minimal fabrication and instrumentation complexity, to enable precise control of flow for efficient mixing and reduced sample consumption, and to allow a direct interface with other components and subsystems to create truly integrated systems. Currently, a majority of lab-on-a-chip systems use passive mixers that rely on molecular diffusion. In particular, passive mixers that are based on electrokinetic transport are of great importance as they are amenable to integration within electrokinetic (EK) microsystems,[2,5] which have attracted widespread interest in the lab-on-a-chip community.

Effective mixing in electrokinetically driven micromixers is difficult because their operations are usually limited to laminar flow and the mixing process is dominated by molecular-diffusion, which generally leads to long channel lengths and mixing times. A number of diffusion-based mixing-enhancing techniques have explored rapid mixing by reducing diffusion distances between individual sample streams. For example, the mixing process can be accelerated by the narrowing (or focusing) of sample streams[6,7] (see Fig. 4 later). Instead of diffusing between broad streams (such as the T-mixer), samples can be arranged in the form of alternating thin streams[8–10] (see Fig. 6 later). Sample concentration profiles in such laminar diffusion-based micromixers are relatively easy to evaluate and reproduce, which also enables other innovative bioanalytical applications by allowing precise handling[11] and dosing[12] of samples, extraction and separation of samples,[13,14] and generation of spatial and temporal concentration gradients.[15–19]

However, there are still important issues regarding these passive mixing techniques that need to be addressed. Optimal design of such mixers involving the tradeoffs among mixer performance, mixing time, chip real-estate area and system complexity is still an art. More extensive exploration of design space to assess the impact of parameters such as mixer topology, element dimension, voltage control, material properties and sample flow ratios has not been pursued. Currently, designers are mostly forced to use trial-and-error approaches that require large numbers of experimental tests or numerical simulations that may involve unacceptably long computation time and algorithmic stability limitations (*e.g.*, accurate simulations of micromixing at high Peclet numbers by finite-volume approaches become very difficult due to errors associated with ''numerical diffusion'',[20] unless extremely fine meshes are used). To address these issues, several analytical modeling efforts have been developed for mixers. Simplified equations for T-mixers[21,22] have been extensively used to provide mixing length estimates that are often overly conservative and does not provide information of the mixing process. Modeling methods using electrical analogy (*i.e.*, resistor-based models)[3,12] assume complete mixing and generally result in unnecessarily long channels. Branebjerg *et al.*[23] have theoretically studied the diffusion behavior in split-and-recombine (SAR) mixers. An analytical solution for the width-wise sample concentration profile within the last unit was developed by neglecting the effects of its preceding SAR units.

[a]*Department of Mechanical Engineering, Carnegie Mellon University, Pittsburgh, Pennsylvania, 15213, USA. E-mail: qlin@andrew.cmu.edu; Fax: +01-412-268-3348; Tel: +01-412-268-3641*
[b]*Department of Electrical and Computer Engineering, Carnegie Mellon University, Pittsburgh, Pennsylvania, 15213, USA*

As such, the model is valid only for the special case that sample concentration distributions at the channel inlet are saw-tooth (interdigitally) shaped, and even so, still requires pre-calculation of flow ratios of different samples. Thus, the model is not suitable for system-oriented simulation and synthesis. Schönfeld *et al.*[24] also derived a formula that accounts for arbitrary sample concentration distributions at channel inlets. However, the formula is limited to symmetric flow ratios (*i.e.*, the flow rates of the buffer streams carrying different samples are the same), and is not applicable to multi-input or multi-output flow intersections that are widely used in focusing and multi-stream mixers.

All the models above are intended for particular instances of micromixers. No general methodology has been proposed to develop a reliable and reusable system-oriented simulation approach that can accommodate all laminar diffusion based micromixers and, most importantly, be integrated with simulations of other subsystems (*e.g.*, reactors, injectors and electrophoretic separation channels). This deficiency hinders efficient microfluidic design, which is typically an iterative process, and becomes even more acute for large-scale microfluidic integration. Therefore, there is a strong need for micromixer design tools that are efficient, accurate, and have general applicability.

To address this need, this paper presents a system-oriented and lumped-parameter approach to modeling laminar diffusion-based passive EK micromixers of complex geometry. Using a simultaneous electric and sample concentration network representation, we decompose complex mixers into a collection of elements of relatively simple geometry. Analytical models for individual elements are derived to accurately describe the variations of sample concentrations. Proper parameters are embedded in these element models to pass electric and sample concentration information from one element to a neighboring element through their interface. As a result, a complex mixer can be represented by a system-level model consisting of individual element models. This system-level model eliminates the need for input parameters that would have to be determined from user-conducted numerical simulations or experiments, and is thus well suited to computed-aided design (CAD) of complex EK micromixers. While focusing on EK micromixers, the concept and methodology of this system-oriented approach can be readily extended to pressure-driven complex micromixers and laminar diffusion-based devices.

2 System-level representation of complex micromixers

A complex electrokinetic passive micromixer can be represented as a system consisting of interconnected mixing elements that have relatively simple geometry. This approach, which applies to passive EK micromixers in general, can be illustrated by an example of a serial mixing network,[12] which consists of reservoirs, microchannels, T- and cross-intersections (Fig. 1). The sample is released and collected by the reservoirs at the extreme ends of the mixer. Within the cross intersection, a portion of the input sample is shunted to channels A_1–A_5 and the rest continues along the flow direction. Using this unit cell repeatedly generates a series of continuously diluted sample concentration in channels A_1–A_5 that can be used for parallel bio-chemical analysis. Variations of buffer and sample concentration profiles are represented by grey levels in Fig. 1a. In our approach, we represent the serial mixing network as a collection of interconnected mixing elements, including microchannels (each with a single input and an output stream of samples or reagents), converging intersections (each with two input and one output streams), and diverging intersections (each with one input and two output streams). We develop parameterized analytical models for mixing processes in these elements by accurately considering the governing electric circuitry and convection–diffusion equations. A system-level model is constructed from models for the constituent elements, which are linked in correspondence to the mixer topology by requiring an appropriate set of parameters (called the interface parameters) to possess continuity at the element interfaces. The system-level model is conveniently represented as a schematic, as shown in Fig. 1b. All element models in such a schematic are parameterized and reusable; and the user can quickly compose and modify the mixer design by wiring these models in an efficient top-down approach. The schematic can be efficiently solved using commercially available CAD simulation tools (*e.g.*, Cadence/Spectre[25]) to evaluate the performance of the resulting design, which offers drastic computational efficiency improvements over full numerical simulations.

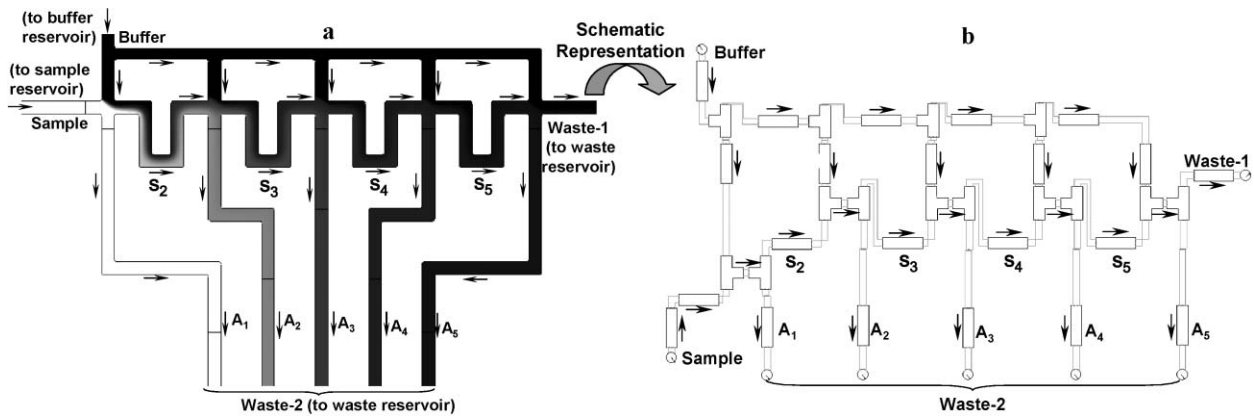

Fig. 1 (a) A complex electrokinetic serial mixing network[12] and (b) its schematic representation for system-level model.

Upon considering the development of element models (Section 3) and interface parameters (Section 4), we will apply, in Section 5, the system-level model to several practically important complex micromixers (including that shown in Fig. 1). The model will be validated by comparing these results to both numerical analysis and experimental data.

3 Element models for system-oriented simulation

This section formulates and solves the circuitry and convection–diffusion equations to yield parameterized and analytical models for mixing elements, including mixing channels, converging and diverging intersections and reservoirs, which are most commonly seen in EK micromixers. The EK motion of the samples consists of two parts: the bulk motion of the carrier buffer due to electroosmosis and the motion of charged sample molecules relative to the buffer due to electrophoresis. We assume the similitude between EK flow and electric field,[26] which implies that the EK velocity of samples can be expressed as $u = \mu E$, where E is the electric field strength and μ is the algebraic sum of the buffer's electroosmotic mobility and sample's electrophoretic mobility in the buffer. The models will be capable of simultaneously simulating multiple dilute samples in the buffer solution if interactions between them can be neglected.

3.1 Tapered mixing channels with small side-wall slope

This subsection formulates the circuitry and convection–diffusion equations for a tapered straight mixing channel with a small side-wall slope. That is, the channel's longitudinal axis (the line connecting cross-sectional centers) is a straight line and its cross sections are rectangular with dimensions varying slowly along the axis. Straight channels are included as a special case of zero side-wall slope. This geometry is employed in micromixers, such as geometric focusing or throttled mixers with side-wall slopes on the order of 10°.[10,27,28] The depth-wise and width-wise dimensions of the channel are defined as those parallel (along the x-axis) and perpendicular (along the y-axis) to the sample stream interface, respectively. Let L, $h(z)$ and $w(z)$ denote the axial length, depth and width of the mixing channel respectively, where z is the longitudinal coordinate parallel to the channel axis.

As the mixing channel is typically narrow ($w/L \ll 1$ and $h/L \ll 1$) and operates in steady state, the axial diffusion of the sample can be neglected and the governing convection–diffusion equation for the sample concentration $c(x, y, z)$ is

$$u_x \frac{\partial c}{\partial x} + u_y \frac{\partial c}{\partial y} + u_z \frac{\partial c}{\partial z} = D\left(\frac{\partial^2 c}{\partial x^2} + \frac{\partial^2 c}{\partial y^2}\right) \quad (1)$$

where D is the sample diffusivity, u_x, u_y and u_z are the x-, y- and z-components of the sample velocity. To solve this equation in a channel with slightly sloped side-walls, we approximate the channel as a set of concatenated channel segments, each having constant rectangular cross sections (Fig. 2a). As a convention, channel segments are numbered $k = 1,2,\ldots N$ from the inlet to the outlet. The interface between segments $k-1$ and k is numbered $k-1$, with the channel inlet numbered 0, and the channel outlet numbered N. Likewise, local coordinates (x_k, y_k, z_k) and dimensions (h_k, w_k, L_k) of segment k can be defined, with h_k and w_k independent of z_k. Other variables or quantities in the kth segment channel are also given the index k.

The electric current induced by very dilute sample molecules are negligible compared with the current in carrier buffer, which is typically valid in EK microfluidic systems.[12,29] Then the electric resistance of the entire channel is given by

$$R = \int_0^L \frac{\mathrm{d}z}{w(z)h(z)\sigma} \quad (2)$$

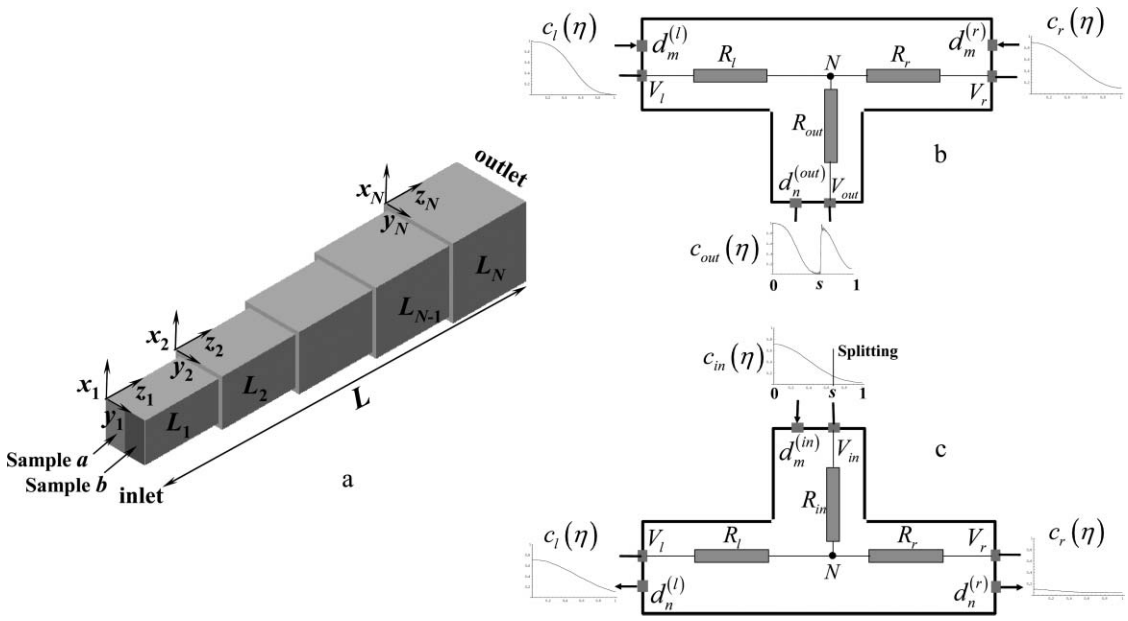

Fig. 2 Sketch for element models: (a) an approximation of the tapered mixing channel by a set of constant-cross section channels, (b) the converging intersection and (c) the diverging intersection.

where σ is the electric conductivity of the buffer solution within the channel. Given a potential difference over the channel length, $\Delta V = V_{in} - V_{out}$ (V_{in} and V_{out} are respectively the voltages at the channel inlet and outlet), eqn. (2) yields the electric current $I = I_k = \Delta V/R$ through the entire channel including all constituent segments. As the slope of the channel's side-wall is small, it is reasonable to use the approximation that the electric field in each channel segment is unidirectional, *i.e.*,

$$(E_{x_k}, E_{y_k}, E_{z_k}) = (0, 0, I/(w_k\, h_k\sigma)) \tag{3}$$

Then EK velocity $\vec{u}_k$ of a sample molecule in segment k is (u_{x_k}, u_{y_k}, u_{z_k}) = (0, 0, μE_{z_k}). That is, within the segment, sample molecules migrate at a velocity that is uniform over the cross section. It follows from eqn. (1) that the sample concentration distribution is two-dimensional and independent of x_k as it is assumed to be so at the channel inlet. This also yields the volumetric flow rate of the buffer stream through a segment: $q_k = u_{eof,z_k}\, h_k w_k = \mu_{eof}\, I/\sigma$, where u_{eof,z_k} and μ_{eof} are the electroosmotic parts of u_{z_k} and μ, respectively. That is, q_k is linearly proportional to the current I. Then, eqn. (1) can be recast in terms of segment coordinates as

$$\frac{w_k^2 u_{z_k}}{D}\frac{\partial c_k}{\partial z_k} = \frac{\partial^2 c_k}{\partial \eta^2} \tag{4}$$

where $\eta = y_k/w_k$ ($0 \leqslant \eta \leqslant 1$) is the normalized coordinate along channel width. With the boundary conditions $\partial c_k/\partial\eta|_{\eta=0,1} = 0$ (*i.e.*, no mass transfer across the walls), the solution to eqn. (4) at the outlet of segment k (interface k) is found as $c_k(\eta, L_k) = \sum_{n=0}^{\infty} d_n^{(k)}(L_k)\cos(n\pi\eta) = \sum_{n=0}^{\infty} d_n^{(k)}(0) e^{-\frac{(n\pi)^2 DL_k}{w_k^2 u_{z_k}}}\cos(n\pi\eta)$, where $d_n^{(k)}(L_k)$ and $d_n^{(k)}(0)$ are the Fourier series coefficients of the concentration profiles at the inlet and outlet of segment k. Noting that the solution is expressed in terms of dimensionless variable η, we have $d_n^{(k)}(0) = d_n^{(k-1)}(L_{k-1})$. Then a complete solution of eqn. (4) is obtained as $d_n^{(k)}(L_k)\Big/ d_n^{(k-1)}(L_{k-1}) = e^{-\frac{(n\pi)^2 DL_k}{w_k^2 u_{z_k}}}$. Letting $k = 1, 2, \ldots$ and taking the product of these equations yields

$$d_n^{(out)} = d_n^{(in)} e^{-(n\pi)^2 D\sum_{k=1}^{N\to\infty}\frac{L_k}{w_k^2 u_{z_k}}} = d_n^{(in)} e^{-(n\pi)^2\gamma\tau} \tag{5}$$

where $d_n^{(out)} = d_n^{(N)}(L_N)$ and $d_n^{(in)} = d_n^{(1)}(0)$ represent the coefficients at the channel inlet and outlet, respectively. Here, $\tau = (L/w(0))/Pe$ is the dimensionless mixing time and $Pe = u(0)\, w(0)/D$ is the Peclet number defined at the channel inlet, which represents the ratio of convective to diffusive transport rates. The geometry factor γ is given by

$$\gamma = \frac{u(0)w(0)^2}{L}\int_0^L \frac{dz}{w^2(z)u(z)} = \frac{1}{L}\int_0^L \frac{h(z)}{h(0)}\frac{w(0)}{w(z)}dz \tag{6}$$

Eqns. (5) and (6) indicate that the variation of sample concentration coefficients within a tapered mixing channel depends on those at the inlet, the dimensionless mixing time and geometry factor γ. Eqn. (5) provides an excellent approximate solution to eqn. (1) when side-wall slopes are small. This will be confirmed with an example in Section 5.2.

Eqn. (5) has been derived for 3D laminar diffusion-based mixing channels. However, 2D mixing channels with variable width but constant depth are widely used (*e.g.*, geometrically focusing mixers[10,20,27,30] and throttled T mixers[28]) and will be discussed primarily in this paper. If w is linear in z with $p = (w(L) - w(0))/w(0)$, then

$$R = \gamma R(0) \text{ and } \gamma = \frac{\ln(1+p)}{p} \tag{7}$$

where $R(0) = L/(w(0)\, h(0)\sigma)$. In addition, for another special case of constant channel cross sectional areas: $h(z)\, w(z) = A = \text{const}$, eqns. (2) and (6) respectively reduce to $R = L/A\sigma$ and $\gamma = \frac{w(0)^2}{L}\int_0^L \frac{dz}{w(z)^2}$, and the solution in ref. 24 is recovered.

3.2 Converging intersections

The converging intersection has two inlets and one outlet, and acts as a combiner to align and compress upstream sample streams of an arbitrary flow ratio s (defined below) and concentration profiles side-by-side at its outlet (Fig. 2b). As its flow path lengths are negligibly small compared with those of mixing channels, such an element can be assumed to have zero physical size, and electrically represented as three resistors with zero resistance between each terminal and the internal node N,

$$R_l = R_r = R_{out} = 0 \tag{8}$$

Here, N corresponds to the intersection of flow paths and the subscripts 'l', 'r' and 'out' represent the left and right inlets, and the outlet, respectively. The voltages at the terminals ($V_l = V_r = V_{out}$) are consequently the same.

The sample concentration profiles, $c_l(\eta)$ and $c_r(\eta)$, at the left and right inlets respectively, can be expressed as $c_l(\eta) = \Sigma_0^\infty d_m^{(l)}\cos(m\pi\eta)$ and $c_r(\eta) = \Sigma_0^\infty d_m^{(r)}\cos(m\pi\eta)$. At the outlet, $c_l(\eta)$ and $c_r(\eta)$ are scaled down to the domains of $0 \leqslant \eta \leqslant s$ and $s \leqslant \eta \leqslant 1$, where $s = q_l/(q_l + q_r) = I_l/(I_l + I_r)$ denotes the interface position (or the flow ratio, the ratio of the left-stream flow rate q_l to the total flow rate $q_l + q_r$) between the incoming streams in the normalized coordinate at the outlet. Note that the flow rates q_l and q_r are respectively linear in the electric currents I_l and I_r as described above, and s can be determined by solving for electric currents within the entire mixer using Kirchhoff's and Ohm's laws. Let $c_{out}(\eta) = \Sigma_0^\infty d_n^{(out)}\cos(n\pi\eta)$ be the concentration profile at the outlet. Then its Fourier coefficients are given by

$$\begin{cases} d_0^{(out)} = d_0^{(l)}s + d_0^{(r)}(1-s) \\ d_{n>0}^{(out)} = s\sum_{m=0}^{m\neq ns} d_m^{(l)}(f_1\sin(f_2) + f_2\sin(f_1))\Big/(f_1 f_2) \\ \qquad + s\sum_{m=0}^{m=ns} d_m^{(l)} + (1-s)\sum_{m=0}^{m=n(1-s)}(-1)^{n-m} d_m^{(r)} \\ \qquad + 2(-1)^n(1-s)\sum_{m=0}^{m\neq n(1-s)} \\ \qquad d_m^{(r)}(\cos(F_2/2)\sin(F_1/2)/F_1 + \cos(F_1/2)\sin(F_2/2)/F_2) \end{cases} \tag{9}$$

where $f_1 = (m - ns)\pi$, $f_2 = (m + ns)\pi$, $F_1 = (m + n - ns)\pi$ and $F_2 = (m - n + ns)\pi$.

3.3 Diverging intersections

A diverging intersection has one inlet and two outlets, and a sample concentration profile coming into the inlet is split and stretched out into two parts exiting the outlets (Fig. 2c). The current in the incoming stream is also split into two. Similar to converging intersections, it is reasonable to assume that diverging intersections have zero physical size, and can be represented by three zero-resistance resistors,

$$R_{\mathrm{in}} = R_{\mathrm{l}} = R_{\mathrm{r}} = 0 \tag{10}$$

which implies equal voltages at the terminals: $V_{\mathrm{in}} = V_{\mathrm{l}} = V_{\mathrm{r}}$. The subscripts 'in', 'l' and 'r' represent quantities at the inlet, the left and right outlets.

Let $c_{\mathrm{in}}(\eta) = \Sigma_0^{\infty} d_m^{(\mathrm{in})} \cos(m\pi\eta)$, $c_{\mathrm{l}}(\eta) = \Sigma_0^{\infty} d_n^{(\mathrm{l})} \cos(n\pi\eta)$ and $c_{\mathrm{r}}(\eta) = \Sigma_0^{\infty} d_n^{(\mathrm{r})} \cos(n\pi\eta)$ be the concentration profiles at the inlet, and left and right outlets, respectively. Then the Fourier coefficients at the outlets are related to those at the inlets by

$$\begin{cases} d_0^{(\mathrm{l})} = d_0^{(\mathrm{in})} + \displaystyle\sum_{m=1}^{\infty} d_m^{(\mathrm{in})} \sin(\phi_1) \Big/ \phi_1 \\ d_{n>0}^{(\mathrm{l})} = 2 \displaystyle\sum_{m=0}^{m\neq n/s} d_m^{(\mathrm{in})} (-1)^{n+1} \phi_1 \sin(\phi_1) \Big/ (f_1 f_2) \\ \qquad + \displaystyle\sum_{m=0}^{m=n/s} d_m^{(\mathrm{in})} \end{cases} \tag{11}$$

$$\text{and} \begin{cases} d_0^{(\mathrm{r})} = d_0^{(\mathrm{in})} - \displaystyle\sum_{m=1}^{\infty} d_m^{(\mathrm{in})} \sin(\phi_1) \Big/ \phi_2 \\ d_{n>0}^{(\mathrm{r})} = 2 \displaystyle\sum_{m=0}^{m\neq n/(1-s)} d_m^{(\mathrm{in})} \phi_2 \sin(\phi_1) \Big/ (F_1 F_2) \\ \qquad + \displaystyle\sum_{m=0}^{m=n/(1-s)} (-1)^{m-n} d_m^{(\mathrm{in})} \end{cases}$$

where $f_1 = (n - ms)\pi$, $f_2 = (n + ms)\pi$, $F_1 = (n + m - ms)\pi$, $F_2 = (n - m + ms)\pi$, $\phi_1 = ms\pi$ and $\phi_2 = m(1 - s)\pi$. Similar to converging intersections, $s = q_{\mathrm{l}}/(q_{\mathrm{l}} + q_{\mathrm{r}}) = I_{\mathrm{l}}/(I_{\mathrm{l}} + I_{\mathrm{r}})$ gives the normalized position of the splitting plane and can be determined by electric current distributions within the network.

3.4 Reservoirs

To enable the system simulation of a mixer, models for sample and waste reservoirs are also needed. A sample reservoir continuously discharges downstream a sample of a given concentration c_0 while providing an electric potential ϕ_{app} to maintain the EK flow. It can thus be simply represented by

$$V = \phi_{\mathrm{app}} \tag{12}$$

and $c(\eta) = \Sigma_0^{\infty} d_n \cos(n\pi\eta)$ where

$$d_0 = c_0 \text{ and } d_{n>0} = 0 \tag{13}$$

A model for a waste reservoir, which provides a fixed electric potential and serves as a sink continuously collecting used samples and reagents, can be given in a similar fashion.

4 Constructing a system-level mixer model from element models

A complex mixer can be modeled by element models developed in Section 3 using the system-oriented approach described in Section 2. The key is to use appropriate parameters to link two element models at their terminals, which correspond to the interface between two neighboring physical mixing elements. Such parameters are illustrated in Fig. 3, which represents a hypothetical system consisting of a straight channel, a converging and a diverging intersection. There are two sets of such interface parameters (represented by pins at each terminal of the element model in Fig. 3): an electric potential $(V_i)^j$, and a set of concentration Fourier coefficients $\{d_n^{(i)}\}^j$ (Section 3), where the index i stands for 'in', 'out', 'l' or 'r', respectively representing the inlet, outlet, left and right

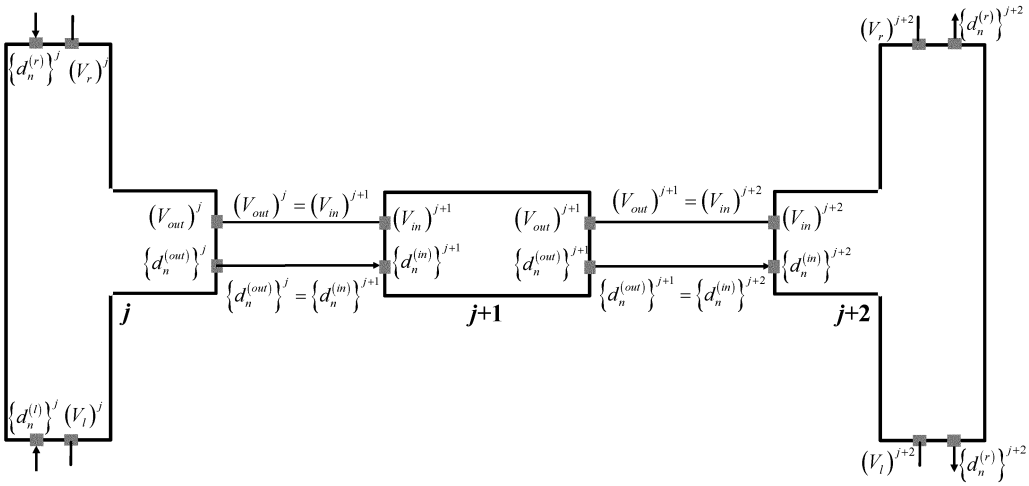

Fig. 3 Linking element models to form a system-level micromixer model.

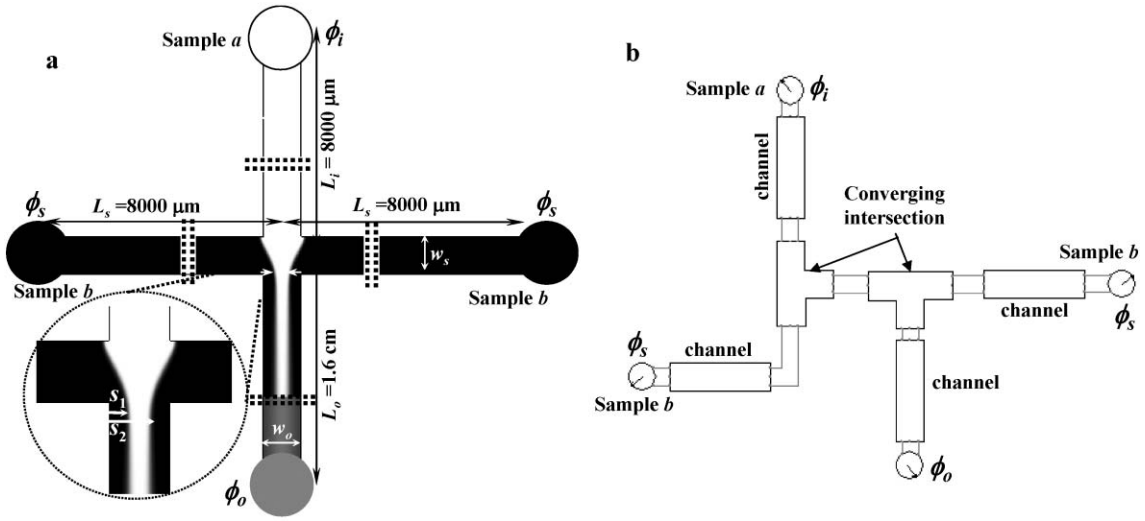

Fig. 4 (a) An electrokinetic focusing micromixer and (b) its schematic representation for system-level modeling.

terminals of the element. The index j is the element number. The parameters between two neighboring elements are set equal, *e.g.*, $(V_{out})^j = (V_{in})^{j+1}$ and $\{d_n^{(out)}\}^j = \{d_n^{(in)}\}^{j+1}$.

This system-oriented simulation approach involves both electric and concentration calculations. First, given the applied potential at the reservoirs, system topology and element geometry, the voltages $(V_i)^j$ at the element terminals are computed for the entire mixer system by Kirchhoff's and Ohm's laws. The electric field strength (E) and its direction within each element, and flow ratios (splitting ratios) at intersections are then calculated. With these results and user-input sample properties (D and μ), the sample speed is given by $u = \mu E$. Next, the concentration coefficients $\{d_n^{(out)}\}^j$ at the outlet(s) of each element j are determined from those at the element's inlet(s) using eqn. (5), (9) and (11), starting from the most upstream sample reservoir (eqn. (13)). As such, both electric and concentration distributions in an EK micromixer are obtained. This would enable efficient and accurate designs of complex micromixers in a top-down and system-oriented fashion.

5 Results and discussion

To demonstrate its utility in lab-on-a-chip design, our system-level model is now applied to several practically important passive electrokinetic mixers. While the system-level model allows for a virtually arbitrary number of different samples coexisting in the buffer, our implementation considered up to three samples, with eqns. (5), (9), (11) and (13) applying to each sample. Ten Fourier terms ($n = 9$) were found to yield sufficient accuracy for concentration simulation.

To validate our model, the system simulation results from the model are compared to both experimental data (serial and parallel mixing networks in Table 1) and full numerical analysis (focusing and multi-stream mixers in Figs. 4 and 6, serial and parallel mixing networks in Table 1). Here, the numerical analysis performed with the commercial finite element-based package FEMLAB 3.0a,[31] solves a full set of electrostatics, incompressible fluid flow and convection–diffusion equations in 2D domains that highly accurately describe the mixing process, and validates the approximate analytical treatment of the full equations by our model. These equations are based on the assumptions of quasi steady-state EK flow, negligible electrical double layer thicknesses, constant channel depths, dilute sample solutions, and identical physicochemical properties (*e.g.*, zeta potential) of channel walls.[32–34]

To characterize the mixing performance, a scalar index, called the mixing residual Q,[10,20,24] is used to quantify the non-uniformity of concentration distributions:

$$Q = \int_0^1 |\bar{c}(\eta) - \bar{c}_{avg}| d\eta \tag{14}$$

where $\bar{c}(\eta) = c/c_0$ and $\bar{c}_{avg} = c_{avg}/c_0$ are the normalized concentration profile and width-averaged concentration, respectively. We assume $c_0 = 1$ in the reservoir without loss of generality. Hence, $c(\eta) = \bar{c}(\eta)$ and $c_{avg} = \bar{c}_{avg}$. Note that a small value of Q indicates a highly homogeneous sample distribution and hence good mixing performance. A smaller difference between $\bar{c}(\eta)$ and $\bar{c}_{avg}$, or a smaller width-wise region occupied by this concentration difference, leads to a lower Q.

For convenience, the following scalar index will be used to characterize the percentage error of our system-level modeling results compared with numerical simulations,

$$M = \frac{\int_0^1 |c_N - c| d\eta}{\int_0^1 c_N d\eta} \tag{15}$$

where c and c_N are the concentration profiles from system-level models and numerical simulations, respectively. For all results below, mixing channels have identical width 200 μm. Also, samples a and b to be mixed (Figs. 5 and 7) are given $D_a = 1 \times 10^{-10}$ m^2 s^{-1}, $D_b = 3 \times 10^{-10}$ m^2 s^{-1} and $\mu_a = \mu_b = 6 \times 10^{-8}$ m^2 V^{-1} s^{-1} unless otherwise noted.

5.1 Electrokinetic focusing mixers

Electrokinetic focusing,[6] which first appeared as a sample injection and manipulation technique[35,36] in EK lab-on-a-chip

systems, also can be utilized to speed up mixing, especially in reaction kinetics studies.[7,37] Such an electrokinetic focusing mixer is illustrated and schematically represented for system-level modeling in Fig. 4. We use subscripts 'i', 's' and 'o' to respectively denote the input, side and output mixing channels. The cross intersection where sample a (white) from the input channel is pinched by buffer or sample b (black) from both side channels, is modeled as two concatenated converging intersections. Therefore, at the mixing channel inlet, two interface positions $s_1 = I_s/(2I_s + I_i)$ and $s_2 = (I_s + I_i)/(2I_s + I_i)$ are obtained if the electric currents from both side channels are identical. Hence, the normalized width occupied by sample a is $s = s_2 - s_1 = I_i/(2I_s + I_i)$. During simulations, voltages (ϕ_s and ϕ_i) are applied at the reservoirs to vary s while keeping E and the sample residence time fixed in the mixing channel. Specifically, $\phi_i = \{240, 267\}$ V, $\phi_s = \{280, 267\}$ V and $\phi_0 = 0$ are chosen to obtain $s = \{0.1, 1/3\}$ with $E = 143$ V cm^{-1}. Fig. 5a shows the comparison of system modeling results and numerical simulations on concentration distributions of samples a and b at the channel outlet. It can be seen that sample b with higher diffusivity mixes much faster and its concentration becomes uniform at the outlet regardless of the initial band width. However for sample a with lower diffusivity, a smaller stream width (*e.g.*, $s = 0.1$) allows more uniform concentration profiles than larger stream widths (*e.g.*, $s = 1/3$). The numerical and system simulation results agree well with a worst-case error of $M = 3\%$ at $s = 0.1$. To gain insight into the mixer performance, the mixing residual Q along the mixing channel is calculated from the system-level model and shown in Fig. 5b. At the channel inlet ($z = 0$), Q, which is the same for both samples due to their complementary concentration profiles ($c_a(\eta) + c_b(\eta) = 1$), strongly depends on s. When the incoming streams are very asymmetric (*e.g.*, $s = 0.1$ or $s = 0.9$), the integral in eqn. (14) yields a lower Q value ($Q = 0.18$ at $s = 0.1$ compared with $Q = 0.44$ at $s = 1/3$) and a more uniform initial profile. Along the channel, Q initially drops rapidly and then becomes saturated because smaller concentration gradients due to improvement in sample mixing reduce the driving force for further mixing. Given sufficient mixing channel lengths, sample concentration profiles will asymptotically approach their averages $c_a(\eta) = I_i/(2I_s + I_i)$ and $c_b(\eta) = 2I_s/(2I_s + I_i)$. It should be noted, however, that this may not be efficient from a design standpoint, as a large increase in channel length would only result in minimal decrease in Q. It can also be seen from Fig. 5b that Q decreases faster for samples of higher diffusivity (*e.g.*, sample b), because of larger τ (dimensionless mixing time) values in eqn. (5). To summarize, asymmetric streams ($s \neq 1/2$) produce more uniform initial profiles and hence focusing is a very useful technique to enhance the mixer performance, provided accompanying decreases in sample detection is tolerable. Within the mixing channel, Q decays faster for the more diffusive (or equivalently less mobile) samples. It is also interesting to point out that in contrast to the T-mixer, the focusing mixer greatly improves sample homogeneity, which can be attributed to the reduced stream width of the samples. That is, as the centerline of the focusing-mixer is effectively an impermeable wall due to symmetry, the diffusion distance between samples is only one-half of the T-mix with the same mixing channel dimensions.

5.2 Multi-stream (inter-digital) micromixers

We now apply our system-level model to electrokinetically driven multi-stream micromixers, which improve mixing by replacing the broad sample streams (such as T-mixer) with alternating, much thinner streams to greatly reduce sample diffusion distances. Depending on the geometry of mixing channels, such mixers can be further divided into those without (Fig. 6a) or with focusing (Fig. 6b). The schematic presentation in Fig. 6c applies to mixers with focusing, and can also be used for mixers without focusing by removing the tapered channel element. In this schematic, samples a (white) and b (black) from two reservoirs are branched by successive diverging intersections into multiple streams. These streams are then arranged to alternate in sample content using feed channels and converging intersections connected in cascade. An inter-digital concentration profile is obtained at the inlet of the mixing channel, in which the streams are mixed. As the feed channels generally do not influence sample mixing downstream, numerical simulations are focused on the sample diffusion process in the mixing channel, with the voltage at the inlet set to a value calculated from the system-level model. The mixers with and without focusing are given the voltage $\phi_i = 198$ and 247 V so that they both have $E = 143$ V cm^{-1} in the uniform mixing channel.

Fig. 7 compares concentration profiles of sample a for both mixers, from the system-level modeling and numerical simulation results, at $z = L_f = L/4$ and $z = L$, where L_f and L are the lengths of the focusing and the entire mixing channels. Excellent agreement between the numerical simulation and system modeling results is observed, with $M = 3\%$ for the case with focusing. Multiple lamination of the sample is clearly seen, and the mixer with focusing facilitates sample diffusion and leads to a highly homogeneous concentration profile. By system simulation, we have observed that Q drops much faster in the mixing channel with focusing than in the one without focusing (not shown), as reduced sample diffusion distances improve mixing efficiency. At $z = L_f = L/4$, a very low mixing residual ($Q = 0.067$) is already achieved for the mixer with focusing. From $z = L/4$ to $z = L$, a modest decrease in Q (from 0.067 to 0.048) is obtained but accounts for about 75% of the total channel length. This implies the inappropriateness of neglecting the appreciable mixing contribution made by the focusing channel.[10,20] In addition, this indicates that shorter mixing channel lengths with less complete, yet still sufficient, mixing may be more cost effective for some applications, demonstrating the utility of our model in optimal choice of mixing channel lengths in mixer design.

5.3 Mixing networks

Finally, our system-level model is well suited to the study of complex mixing networks,[12] in which different sample concentrations can be obtained at multiple output channels by geometrically repeating units with a single constant voltage applied at all sample and buffer reservoirs. Here we apply the model to the serial mixing network (Fig. 1) described in Section 2. The system modeling results, along with numerical simulations and experimental data, are presented in Table 1, which lists sample (rhodamine B) concentrations in analysis

Table 1 Comparison of system modeling results (sys) with numerical (num) and experimental (exp) data on sample concentrations in analysis channels of serial and parallel mixing networks

Serial mixing network						Parallel mixing network			
Complete mixing				Partial mixing			Complete mixing		
Channel	c (sys)	c (exp)	c (num)	c (sys)	c (num)	Channel	c (sys)	c(exp)	c (num)
A_1	1	1	1	1	1	A_1	0	0	0
A_2	0.37	0.36	0.378	0.48	0.496	A_2	0.83	0.84	0.832
A_3	0.22	0.21	0.224	0.187	0.187	A_3	0.68	0.67	0.674
A_4	0.125	0.13	0.133	0.081	0.0815	A_4	0.52	0.51	0.523
A_5	0.052	0.059	0.0628	0.029	0.0315	A_5	0.35	0.36	0.354
						A_6	0.17	0.19	0.168
						A_7	1	1	1

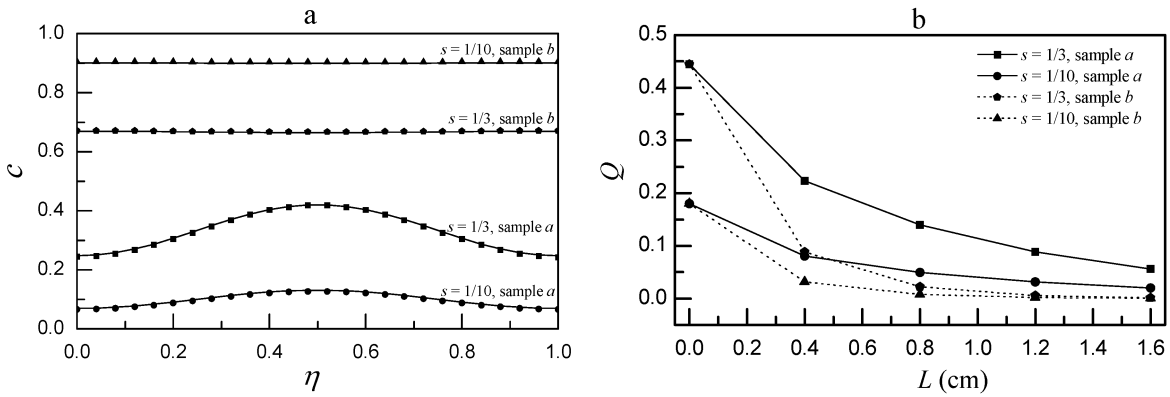

Fig. 5 (a) System modeling results (lines) compared with numerical data (symbols) on concentration profiles for the electrokinetic focusing micromixer. (b) System modeling results on the variation of the mixing residual along the channel length (data points are connected by lines to guide the eye) for the electrokinetic focusing micromixer.

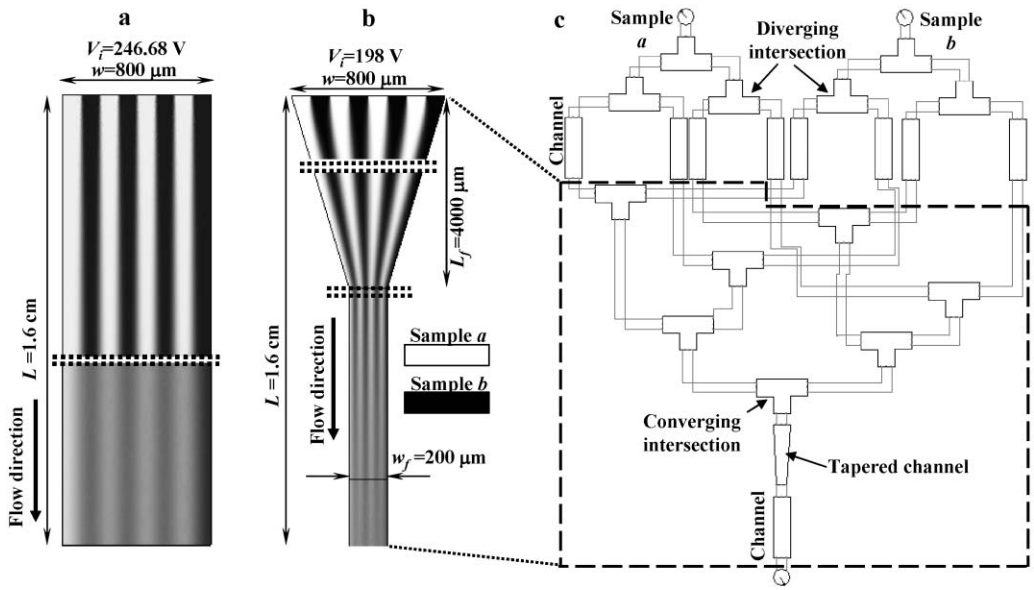

Fig. 6 Multi-stream micromixers (a) without or (b) with focusing and (c) their schematics.

channels A_1–A_5. Both nearly complete and partial mixing situations are analyzed. When a voltage of $\phi_{app} = 0.4$ kV is applied to the sample and buffer reservoirs with the waste reservoirs grounded, sample mixing in channels S_2–S_5 is nearly width-wisely complete (with $Q = 0.007$ at the end of channel S_2). As a result, sample concentrations in channels A_1–A_5 are independent of sample properties and determined *only* by the electric currents in the mixing network. There is excellent agreement of the system-level model with numerical simulations and experimental data (with an average error smaller

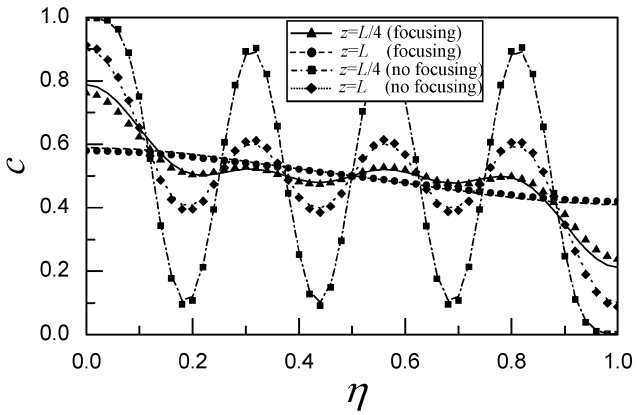

Fig. 7 System modeling results (lines) are compared with numerical data (symbols) on concentration profiles (sample *a*) at $z = L_f$ and $z = L$ for the electrokinetic multi-stream micromixer.

than 6%). It is also interesting to note that in contrast to electric resistor-based models[3,12] that require post-calculations of concentrations from distributions of electric currents in the network, our model directly yields concentration values.

In addition to complete mixing, partial mixing in which the sample concentrations in channels S_2–S_5 are not width-wise uniform and hence the resistor-based modeling is not valid, can be readily modeled with our system-level model. In this case, sample concentrations in channels A_1–A_5 depend not only on electric currents in the network but also the sample concentration profiles at the exit of channels S_2–S_5. Results from our system-level model are also listed in Table 1. While a lack of knowledge of sample properties does not allow experimental data to be used for comparison, these system modeling results are compared with numerical simulations, assuming a diffusivity of $D = 3 \times 10^{-10}$ m^2 s^{-1} and an EK mobility of $\mu = 2.0 \times 10^{-8}$ m^2 V^{-1} s^{-1}. A voltage of $\phi_{app} = 1.6$ kV, as used in experiments in the literature,[12] is applied to the sample and buffer reservoirs, with the waste reservoirs grounded. Good agreement can be observed, with an average error of 4%. From the table, we can observe that as a result of high ϕ_{app}, which is four times that used in the nearly complete mixing case above, there is a four-fold increase in EK velocity and decrease in sample residence time in the channels. Therefore, mixing in channels S_2–S_5 is incomplete (with $Q = 0.14$ at the end of channel S_2). At the cross-intersection following channel S_2, the amount of sample shunted to A_2 is more than that predicted by the complete-mixing based resistor-model due to non-uniform sample distributions at the intersection's inlet (Fig. 1). Consequently, concentrations in channels A_3–A_5 have lower values, agreeing with experimental observations.[12]

Parallel mixing networks[4] can be represented and simulated in a similar fashion. In such a network, all the channels are designed with similar cross-sectional area. Thus, at the T-intersections (T_2–T_6) the currents from the sample and buffer reservoirs are inversely proportional to the length (Ohm's law) of their feed channels (B_1–B_6 and S_2–S_7), given a single constant voltage (1 kV) applied to all sample and buffer reservoirs. Therefore, through proper choice of the lengths of those feed channels, an array of different sample concentrations can be eventually obtained in the output channels (A_1–A_7). Fig. 8 illustrates the schematic representation of the parallel mixing network. Comparisons of system modeling

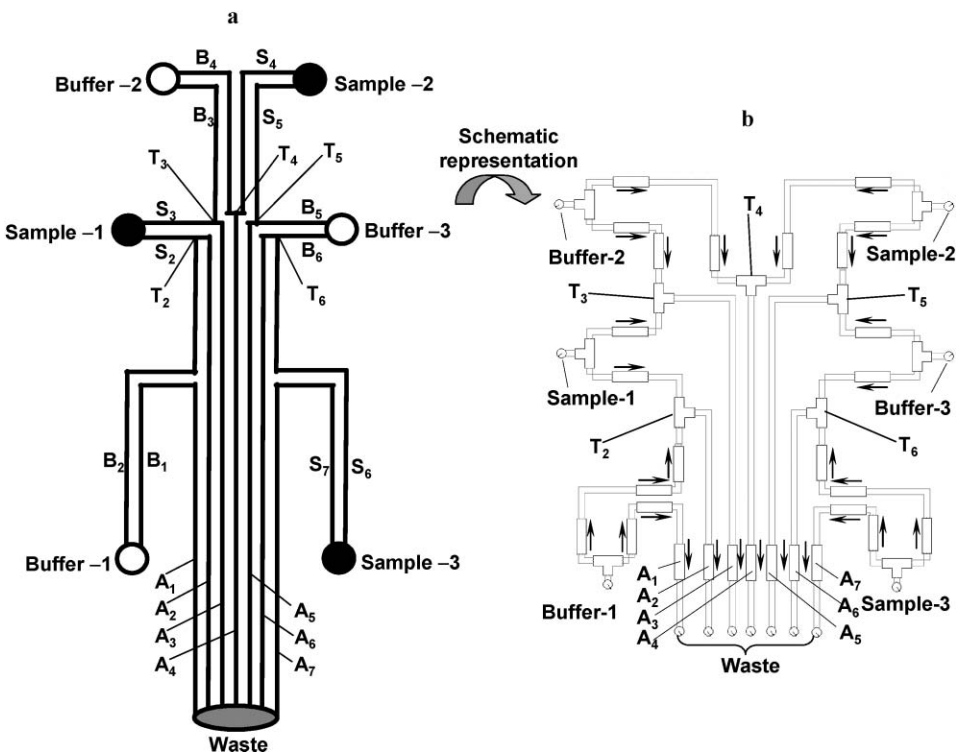

Fig. 8 A complex electrokinetic parallel mixing network[12] and its schematic representation for system-oriented simulation.

results with experimental data and numerical simulations are shown in Table 1. An average error of 3.6% relative to experiments is found.

Finally, it is interesting to note that our system-level model has demonstrated drastic improvement in computational efficiency over the full numerical simulations. For example, on a multi-user 2-CPU 1-GHz Sun Fire 280 processors with 4 GB RAM, using Cadence's[25] integrated circuit design tool for schematic entry and netlisting the system topology from the schematic editor into a text file readable by the simulator (Spectre[25]), the system-oriented simulations of the serial mixing network above were completed within 20 s with netlisting and less than 1 s without netlisting. In contrast, using the same computational platform, 6 h was needed to complete the computation of a numerical model in FEMLAB 3.0a,[31] which were not reusable when chip topologies and dimensions were modified. The computational advantage of our system model is thus clear, making possible system-oriented optimal design that may involve hundreds or thousands of iterative simulations.

6 Conclusions

We have presented an efficient and accurate approach to modeling sample mixing in laminar diffusion-based electrokinetic passive mixers and mixing networks. Complex micromixers are decomposed into a system of elements with relatively simple geometry. Fully parameterized and analytical element models are obtained, which are linked to form a system-oriented representation of the entire micromixer. The resulting system model is verified with numerical simulations and experimental data, and used to perform systematic analysis and comparison of sample mixing in focusing, multi-stream and complex mixing network devices, yielding insights into the effects of such parameters as system topology, geometry, properties and operational parameters on mixing performance. The model affords drastically improved computational efficiency over numerical simulations, and is thus well suited for optimal microchip design processes that typically involve large numbers of design iterations.

Parameterized and analytical models for elements are the building blocks of our system-level model. We consider four types of basic elements: mixing channels, diverging and converging intersections and reservoirs. Such elements are amenable to analytical modeling and are sufficiently general to represent electrokinetic laminar diffusion-based passive micromixers commonly used in lab-on-a-chip systems. The models developed for these elements are valid for general input concentration profiles and arbitrary flow ratios, and enable us to consider for the first time the overall effects of complex mixer topology, geometry, operational parameters and material properties at the system level.

The system-level model represents a general passive mixer in terms of models for the constituent elements. The communication between adjacent elements is enabled through a proper choice of the interface parameters, which include electric potential V and Fourier coefficients of sample concentration $\{d_n\}$. The system-oriented representation has been implemented in an efficient simulation framework allowing fast iterative design processes that would be otherwise time-consuming and expensive.

The system model has been used to perform systematic studies of electrokinetic passive micromixers that employ diffusion-based mixing-enhancing techniques such as focusing, multi-lamination and their combinations. These techniques are effective in improving mixing performance but lead to complex mixer geometries, an extensive and sensitive design-parameter space and complicated design processes. Generally, system-oriented simulations demonstrate that asymmetric sample flow rates should be used for improved mixing efficiency as long as the sample concentrations remain at a detectable level. Sample homogeneity improves rapidly at the early stage of mixing but then tends to saturate eventually, with the region in which this transition occurs determined by the mixer topology and geometry, operational parameters (*e.g.*, flow ratios) and material properties. Therefore, the tradeoff among the chip real-estate area, mixing time, and system complexity should be considered. A salient advantage offered by our system-level model over the resistor-based model is its capability of computing the complex mixing network that involves partial mixing. Therefore, our system-level model can be a useful tool to design more compact mixer topologies.

It is worth noting that while the system-level model focuses on electrokinetic micromixers, the conceptual approach can be generalized to micromixers that use pressure-driven flow. In particular, the model can be directly applied, with minor modifications, to pressure-driven mixers consisting of mixing channels with relatively large width-to-depth ratios.[9,10] In such a thin channel, the diffusion process can be regarded as two-dimensional,[38–41] with the pressure and mean flow velocity playing the roles of electric potential and EK velocity. The effects of non-uniform buffer velocity profiles along the channel depth on sample mixing can be characterized by a stream-wise Taylor dispersion coefficient.[39–41] Additionally, another alternative and simplified model neglecting the stream-wise dispersion is also available and extensively used,[15,38] although with slightly decreased accuracy at high Peclet numbers.[39–41] In the case of pressure-driven mixers using channels of smaller width-to-depth ratios, closed-form correlations might be obtained from a combination of the analytical approach and numerical simulations. This extension will be pursued in future work to allow efficient and accurate design of complex micromixers for applications using pressure-driven flow, for example concentration gradient generators[16] for cell analysis and micro-fabrication, and diffusion-based sample extractors or filters.[13] Additionally, future work will also address the integration of the system-level mixer model with models for other functional microfluidic components, such as injectors, electrophoretic separation systems and reactors. This would form a higher-system-level model for a complete electrokinetic lab-on-a-chip,[3] and enable accurate and efficient simulation of complex, integrated and multi-functional lab-on-a-chip systems.[42]

Acknowledgements

This research is sponsored by DARPA and Air Force Research Laboratory, Air Force Material Command, USAF,

under grant number F30602-01-2-0587, and the NSF ITR program under award number CCR-0325344.

References

1 D. R. Reyes, D. Lossifidis, P.-A. Auroux and A. Manz, Micro total analysis systems. 1. Introduction, theory, and technology, *Anal. Chem.*, 2002, **74**, 2623–2636.

2 P. A. Aurouz, D. Lossifidis, D. R. Reyes and A. Manz, Micro total analysis systems. 2. Analytical standard operations and applications, *Anal. Chem.*, 2002, **74**, 2637–2652.

3 N. H. Chiem and D. J. Harrison, Microchip systems for immunoassay: an integrated immunoreactor with electrophoretic separation for serum theophylline determination, *Clin. Chem.*, 1998, **44**, 591–598.

4 S. B. Cheng, C. D. Skinner, J. Taylor, S. Attiya, W. E. Lee, G. Picelli and D. J. Harrison, Development of a multichannel microfluidic analysis system employing affinity capillary electrophoresis for immunoassay, *Anal. Chem.*, 2001, **73**, 1472–1479.

5 L. Bousse, C. Cohen, T. Nikiforov, A. Chow, A. R. Kopf-Sill, R. Dubrow and J. W. Parce, Electrokinetically controlled microfluidic analysis systems, *Annu. Rev. Biophys. Biomol. Struct.*, 2000, **29**, 155–181.

6 S. C. Jacobson and J. M. Ramsey, Electrokinetic focusing in microfabricated channel structures,, *Anal. Chem.*, 1997, **69**, 3212–3217.

7 J. B. Knight, A. Vishwanath, J. P. Brody and R. H. Austin, Hydrodynamic focusing on a silicon chip: mixing nanoliters in microseconds, *Phys. Rev. Lett.*, 1998, **80**, 3863–3866.

8 L. M. Fu, R. J. Yang, C. H. Lin and Y. S. Chien, A novel microfluidic mixer utilizing electrokinetic driving forces under low switching frequency, *Electrophoresis*, 2005, **26**, 1814–1824.

9 M. Koch, D. Chatelain, A. G. R. Evans and A. Brunnschweiler, Two simple micromixers based on silicon, *J. Micromech. Microeng.*, 1998, **8**, 123–126.

10 P. Löb, K. S. Drese, V. Hessel, S. Hardt, C. Hofmann, H. Lowe, R. Schenk, F. Schonfeld and B. Werner, Steering of liquid mixing speed in interdigital micro mixers—from very fast to deliberately slow mixing, *Chem. Eng. Technol.*, 2004, **27**, 340–345.

11 L. M. Fu, R. J. Yang, G. B. Lee and Y. J. Pan, Multiple injection techniques for microfluidic sample handling, *Electrophoresis*, 2003, **24**, 3026–3032.

12 S. C. Jacobson, T. E. McKnight and J. M. Ramsey, Microfluidic devices for electrokinetically driven parallel and serial mixing, *Anal. Chem.*, 1999, **71**, 4455–4459.

13 B. H. Weigl and P. Yager, Microfluidics—Microfluidic diffusion-based separation and detection, *Science*, 1999, **283**, 346–347.

14 A. Hatch, E. Garcia and P. Yager, Diffusion-based analysis of molecular interactions in microfluidic devices, *Proc. IEEE*, 2004, **92**, 126–139.

15 M. A. Holden, S. Kumar, E. T. Castellana, A. Beskok and P. S. Cremer, Generating fixed concentration arrays in a microfluidic device, *Sens. Actuators, B*, 2003, **92**, 199–207.

16 N. L. Jeon, S. K. W. Dertinger, D. T. Chiu, I. S. Choi, A. D. Stroock and G. M. Whitesides, Generation of solution and surface gradients using microfluidic systems, *Langmuir*, 2000, **16**, 8311–8316.

17 S. K. W. Dertinger, D. T. Chiu, N. L. Jeon and G. M. Whitesides, Generation of gradients having complex shapes using microfluidic networks, *Anal. Chem.*, 2001, **73**, 1240–1246.

18 F. Lin, W. Saadi, S. W. Rhee, S. J. Wang, S. Mittal and N. L. Jeon, Generation of dynamic temporal and spatial concentration gradients using microfluidic devices, *Lab Chip*, 2004, **4**, 164–167.

19 S. J. Wang, W. Saadi, F. Lin, C. M. C. Nguyen and N. L. Jeon, Differential effects of EGF gradient profiles on MDA-MB-231 breast cancer cell chemotaxis, *Exp. Cell Res.*, 2004, **300**, 180–189.

20 S. Hardt and F. Schönfeld, Laminar mixing in different interdigital micromixers: II. Numerical simulations, *AIChE J.*, 2003, **49**, 578–584.

21 N.-T. Nguyen and S. T. Wereley, *Fundamentals and applications of microfluidics*, Artech House, Boston, MA, 2002.

22 T. T. Veenstra, T. S. J. Lammerink, M. C. Elwenspoek and A. van den Berg, Characterization method for a new diffusion mixer applicable in micro flow injection analysis systems, *J. Micromech. and Microeng.*, 1999, **9**, 199–202.

23 J. Branebjerg, P. Gravesen, J. P. Krog and C. R. Nielsen, Fast mixing by lamination, *Proc. IEEE-Micro Electro Mech. Syst. '96*, 1996, 441–446.

24 F. Schönfeld, K. S. Drese, S. Hardt, V. Hessel and C. Hofmann, Optimized Distributive micro-mixing by 'chaotic' multilamination, *Proceedings of Modeling and Simulation of Microsystems (MSM'04)*, Boston, MA, pp. 378–381, 2004.

25 http://www.cadence.com.

26 E. B. Cummings, S. K. Griffiths, R. H. Nilson and P. H. Paul, Conditions for similitude between the fluid velocity and electric field in electroosmotic flow, *Anal. Chem.*, 2000, **72**, 2526–2532.

27 V. Hessel, S. Hardt, H. Lowe and F. Schonfeld, Laminar mixing in different interdigital micromixers: I. Experimental characterization, *AIChE J.*, 2003, **49**, 566–577.

28 D. Gobby, P. Angeli and A. Gavriilidis, Mixing characteristics of T-type microfluidic mixers, *J. Micromech. Microeng.*, 2001, **11**, 126–132.

29 C. X. Qiu and D. J. Harrison, Integrated self-calibration via electrokinetic solvent proportioning for microfluidic immunoassays, *Electrophoresis*, 2001, **22**, 3949–3958.

30 K. S. Drese, Optimization of interdigital micromixers via analytical modeling—exemplified with the SuperFocus mixer, *Chem. Eng. J.*, 2004, **101**, 403–407.

31 http://www.comsol.com.

32 S. V. Ermakov, S. C. Jacobson and J. M. Ramsey, Computer simulations of electrokinetic transport in microfabricated channel structures, *Anal. Chem.*, 1998, **70**, 4494–4504.

33 *FEMLAB 3.0: Chemical Engineering Module Model Library*, pp. 144–156, 2004.

34 L. Q. Ren, D. Sinton and D. Q. Li, Numerical simulation of microfluidic injection processes in crossing microchannels, *J. Micromech. Microeng.*, 2003, **13**, 739–747.

35 S. C. Jacobson, R. Hergenroder, L. B. Koutny, R. J. Warmack and J. M. Ramsey, Effects of Injection Schemes and Column Geometry on the Performance of Microchip Electrophoresis Devices, *Anal. Chem.*, 1994, **66**, 1107–1113.

36 S. C. Jacobson, R. Hergenroder, L. B. Koutny and J. M. Ramsey, High-Speed Separations on a Microchip, *Anal. Chem.*, 1994, **66**, 1114–1118.

37 P. S. Dittrich, B. Muller and P. Schwille, Studying reaction kinetics by simultaneous FRET and cross-correlation analysis in a miniaturized continuous flow reactor, *Phys. Chem. Chem. Phys.*, 2004, **6**, 4416–4420.

38 A. E. Kamholz, B. H. Weigl, B. A. Finlayson and P. Yager, Quantitative analysis of molecular interaction in a microfluidic channel: The T-sensor, *Anal. Chem.*, 1999, **71**, 5340–5347.

39 D. A. Beard, Taylor dispersion of a solute in a microfluidic channel, *J. Appl. Phys.*, 2001, **89**, 4667–4669.

40 K. D. Dorfman and H. Brenner, Comment on "Taylor dispersion of a solute in a microfluidic channel" [*J. Appl. Phys.*, 2001, **89**, 4667], *J. Appl. Phys.*, 2001, **90**, 6553–6554.

41 D. A. Beard, Response to "Comment on 'Taylor dispersion of a solute in a microfluidic channel' [*J. Appl. Phys.*, 2001, **90**, 6553]", *J. Appl. Phys.*, 2001, **90**, 6555–6556.

42 Y. Wang, R. M. Magargle, Q. Lin, J. F. Hoburg and T. Mukherjee, System-Oriented Modeling and Simulation of Biofluidic Lab-on-a-Chip, *Proceedings of the 13th International Conference on Solid-State Sensors, Actuators and MicroSystems*, Seoul, Korea, 2005, pp. 1280—1283.